Brief communication: Surface energy balance differences over Greenland between ERA5 and ERA-Interim

Uta Krebs-Kanzow[1], Christian B. Rodehacke[1,2], and Gerrit Lohmann[1,3]

[1]Alfred-Wegener-Institut, Helmholtz-Zentrum für Polar- und Meeresforschung, Bremerhaven, Germany
[2]Danish Meteorological Institute, Copenhagen, Denmark
[3]University of Bremen, Bremen, Germany

Correspondence: Uta Krebs-Kanzow (uta.krebs-kanzow@awi.de)

Abstract. We compare the main atmospheric drivers of the melt season over the Greenland Ice Sheet (GrIS) in ERA5 and ERA-Interim (ERAI) in their overlapping period 1979–2018. In summer, ERA5 differs significantly from ERAI, especially in the melt regions. Small scale ERA5- ERAI differences near the ice sheet's margins and over steep slopes can be explained by the different resolution while the large scale differences indicate a different representation of physical processes in the two reanalyses: Averaged over the lower parts of the GrIS, mean near-surface air temperature is $1\,\mathrm{K}$ lower, while the mean downward shortwave radiation at the surface is on average $15\,\mathrm{Wm^{-2}}$ higher than in ERAI. Comparison with observational weather station data shows a significant warm bias in ERAI and for ERA5 a significant positive bias in downward shortwave radiation. Consequently, methods that previously estimated the GrIS surface mass balance from the ERAI surface energy balance need to be carefully recalibrated before converting to ERA5 forcing.

1 Introduction

Greenland summer temperatures are experiencing a persistent positive trend. In coastal instrumental temperature records, Hanna et al. (2021) diagnose a significant $1.7\,\mathrm{K}$ increase from 1991 to 2019, and an ensemble mean of SSP5-8.5 projections yields a warming of 5.3 K from the first to the last two decades of the 21st century. Considering a wider range of scenarios, projections generally indicate warming over Greenland, which is weaker than across the remaining Arctic, slightly stronger than the global trends, and mostly comparable to trends over northern hemisphere land surfaces (Climate Change , IPCC, Fig. 4.19). The associated increase in surface melt and runoff leads to a reduction in the GrIS SMB that ultimately raises the global sea level. According to the conservative estimate of Hanna et al. (2021), the equivalent sea level rise amounts to more than $10\,\mathrm{cm}$ by the end of this century for the SSP5-8.5 scenario. Surface mass and energy balance models (EBMs hereafter), such as BESSI (Born et al., 2019) or dEBM (Krebs-Kanzow et al., 2021), represent the key physical processes that determine the surface mass balance, and they can be used to directly infer changes in SMB from basic surface climate variables which typically include surface downward shortwave and longwave radiation, near-surface air temperature, and precipitation.

EBMs provide a low-cost alternative to computationally intensive regional climate model simulations to downscale the SMB and reproduce the narrow ablation zone along the lower elevated ice sheet margins. In a model intercomparison (Fettweis et al., 2020), EBMs were shown to be able to reconstruct the 1979–2012 SMB of the GrIS from relatively coarse-resolution ERA-

Interim climate reanalysis, even though EBMs proved to be somewhat less skillful than regional climate models (RCMs), which may be partly related to the relatively coarse resolution of the ERA-Interim forcing (approximately $79\,\mathrm{km}$) compared to the higher resolution of participating RCMs of up to $5.5\,\mathrm{km}$. However, ERA-Interim was suspended in 2018 and is replaced by the ongoing ERA5 reanalysis product, which provides higher horizontal resolution (approximately $30\,\mathrm{km}$) and dates further back to 1959. Thus, the potential and relevance of EBMs have increased when used in combination with this higher-resolution climate forcing now available.

It is, therefore, desirable to update current SMB simulations based on EBMs to ERA5 forcing and, where necessary, to adjust existing EBM parameters, which will require an assessment of the differences between the two data products due to changes in the near-surface radiation scheme, cloud scheme, or surface boundary layer. To this end, we compare key climate properties between ERA5 and ERA-Interim to complement previous comparisons (Wang et al., 2019; King et al., 2022; Delhasse et al., 2020) focussing on the Greenland (summer) surface energy balance.

2 Data and method

We use two global atmospheric reanalysis datasets produced by the European Centre for Medium-Range Weather Forecasts (ECMWF). The ECMWF Reanalysis - Interim (ERA-Interim, henceforth ERAI) covers the period from January 1979 to August 2019 and has a spatial resolution of about $80\,\mathrm{km}$ with 60 vertical levels over Greenland. The more recent ECMWF Reanalysis v5 (ERA5) begins in January 1940, runs until the present, and has a finer resolution of about $30\,\mathrm{km}$ with 137 vertical levels. We compare climate properties that primarily control surface ablation over the Greenland Ice Sheet (GrIS) for those years entirely covered by both the ERA-Interim and ERA5 data sets, namely the joint period 1979–2018. Specifically, we compare the 2m-air temperature (T2m), downward shortwave radiation at the surface (SWD), effective atmospheric emissivity (ϵ), and downward longwave radiation at the surface (LWD).

The analysis focuses on the summer months (June, July, and August; hereafter JJA) and the lower parts of the ice sheets between sea level and $2000\,\mathrm{m}$ elevation. The effective atmospheric emissivity ϵ is derived from the LWD and $T2m$ according to the Stefan-Boltzmann-Law:

$$\epsilon = \frac{LWD}{\sigma\,T2m_{int}^4} \tag{1}$$

where σ is the Stefan-Boltzmann constant.

For these variables, we analyse mean differences (Fig. 1) and standard deviations (Fig. S1 in the supplement) of corresponding ERA5 - ERAI differences for the summers in the 1979–2018 overlap period. A corresponding comparison of the annual fields can be found in the supplement (Fig. S2, S3). All climate variables considered were bilinearly interpolated to the $1\,\mathrm{km}$ grid used by the Ice Sheet Model Intercomparison Project for CMIP6 (ISMIP6); (Note that effective emissivity is calculated from the coarse resolution LWD and T2m and then interpolated).

We also scale temperatures with respect to a common orography, the $1\,\mathrm{km}$ ISMIP6 orography H_{ice} (Morlighem et al., 2014), to reduce those temperature differences which are related to differences in topography between both reanalyses (resulting from

the higher horizontal resolution in ERA5). To this end, a lapse rate of $\gamma = -0.005 \, \text{K m}^{-1}$ is applied to adjust ERA5 and ERAI 2m-air temperatures:

$$T2m = T2m_{int} + \gamma(H_{ice} - H_{int}) \tag{2}$$

60 where $T2m_{int}$ and H_{int} are the interpolated near-surface air temperature and surface elevation from the respective reanalysis data sets (i.e., ERA5 or ERA-Interim). The applied lapse rate is at the low end of summer lapse rates over Greenland slopes estimated from ERA5 and ERA-Interim 2m-air temperatures, which typically vary between $-5 \, \text{K km}^{-1}$ and $-7 \, \text{K km}^{-1}$ (Fig. S4) in agreement with climate simulations (Erokhina et al., 2017). A comparison of the mean T2m ERA5-ERAI biases for different lapse rate choices ($0 \, \text{K km}^{-1}$, $-5 \, \text{K km}^{-1}$, $-7 \, \text{K km}^{-1}$, $-10 \, \text{K km}^{-1}$) is provided in the supplement (Fig. S5, S6)

65 To also compare the reanalysis data to observational data, we bilinearly interpolate T2m, SWD, and emissivity (ϵ) and LWD from the $1 \, \text{km}$ grid to locations of automatic weather stations (AWS) from the PROMICE network (Fausto et al., 2021; Ahlstrom et al., 2008). We consistently apply the lapse rate correction of $-5 \, \text{K km}^{-1}$ to downscale T2m to the altitude of the weather stations and compare it to monthly mean near-surface air temperature measurements. A comparison with uncorrected temperatures is given in the supplement (Fig. S7). This comparison with observational data is similar, but not identical, to

70 parts of Delhasse et al. (2020) because we use a different interpolation strategy and apply a lapse rate correction to account for altitude differences.

3 Differences between ERA5 and ERAI in summer

During the summer months, ERA5 and ERAI exhibit pronounced differences in the variables considered (Fig. 1). Over the entire 40-year period, mean summer 2m-air temperatures (T2m) in ERA5 are more than $1 \, \text{K}$ lower than in ERAI over most

75 parts of the ice sheet except the South Eastern margins and the southern dome region. The mean bias exceeds two standard deviations of the interannual variability almost everywhere north of $66°N$. The applied lapse rate correction of $-5 \, \text{K km}^{-1}$ appears to be well chosen as the spatial difference between the two reanalysis products increases when no lapse rate correction is applied, or a higher lapse rate of $-10 \, \text{K km}^{-1}$ is chosen (Fig. S5).

The summer shortwave downward radiation at the surface (SWD) is larger in ERA5 than in ERAI over the main ice sheet.

80 The mean bias exceeds two standard deviations on the lower parts of the ice sheet where SWD in ERA5 exceeds SWD in ERAI by approximately $15 \, \text{W m}^{-2}$. Only isolated ice caps and the outermost margins of the main ice sheet show a distortion of the opposite sign in some places. Downward longwave radiation over lower parts of the ice sheet is lower in ERA5 which, in most parts, seems to be related to the lower temperature while atmospheric emissivity shows no remarkable change. An exception is the central-eastern margin where lower LWD is related to a pronounced negative bias in effective atmospheric

85 emissivity and points to a qualitatively different climate regime (here the mean bias in emissivity and LWD exceeds two standard deviations between $66°N$ and $70°N$). Finally, neither difference in longwave nor in shortwave radiation are associated with a correspondingly different cloud cover in ERA5 (Fig. S8 in the Supplement).

A comparison with automatic weather station (AWS) measurements from the PROMICE network (Fausto et al., 2021; Ahlstrom et al., 2008) (Fig. 2) shows no significant bias in the ERA5 summer temperatures while the ERAI summer temper-
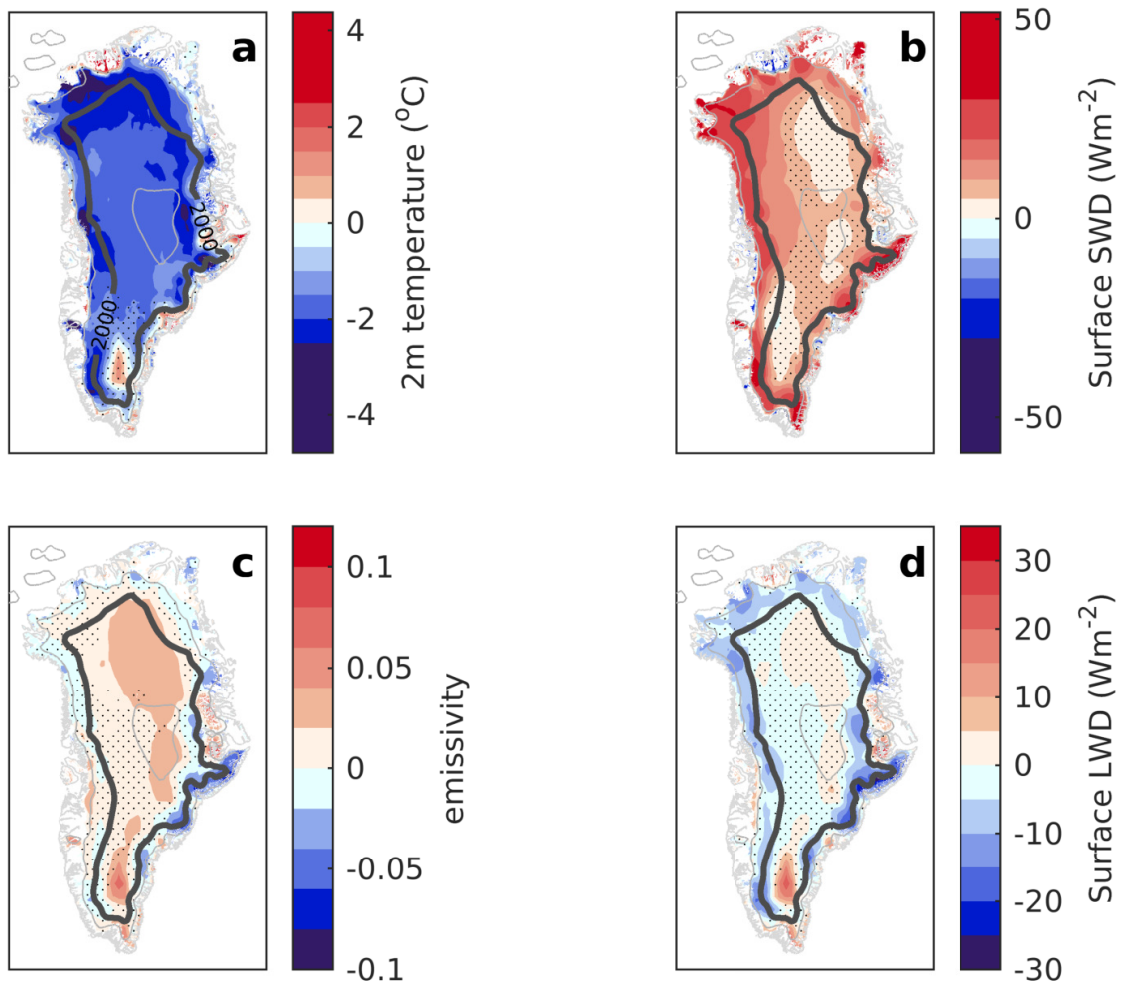
Figure 1. Mean bias between ERA5 and ERAI for the summer mean (i.e., June, July, and August, JJA) 1979–2018 period of the lapse rate corrected 2m-air temperature (top left), downward shortwave radiation (top right), emissivity (bottom left) and downward longwave radiation (bottom right). Stippling indicates regions where the mean bias is smaller than two respective standard deviations. The solid gray line depicts the elevation of 2000 m.

atures are significantly higher than the observations with a mean bias of $0.74\,\mathrm{K}$ (according to t-tests with a 0.05 significance level). Here again a lapse rate correction of $5\,\mathrm{K\,km^{-1}}$ was applied to correct for elevation differences between the interpolated reanalysis data and the elevation of the AWS. A comparrison with uncorrected temperatures reveals that the lapse rare correction reduces the spread of the reanalysis data around the observational data considerably but also reinforces the warm bias in ERAI (Fig. S7). Fig. 2) also shows a larger scatter in SWD around observed station data, a significant positive bias in SWD for ERA5, and a significant negative bias in emissivity and LWD for both reanalyses. There is no significant bias in the ERAI
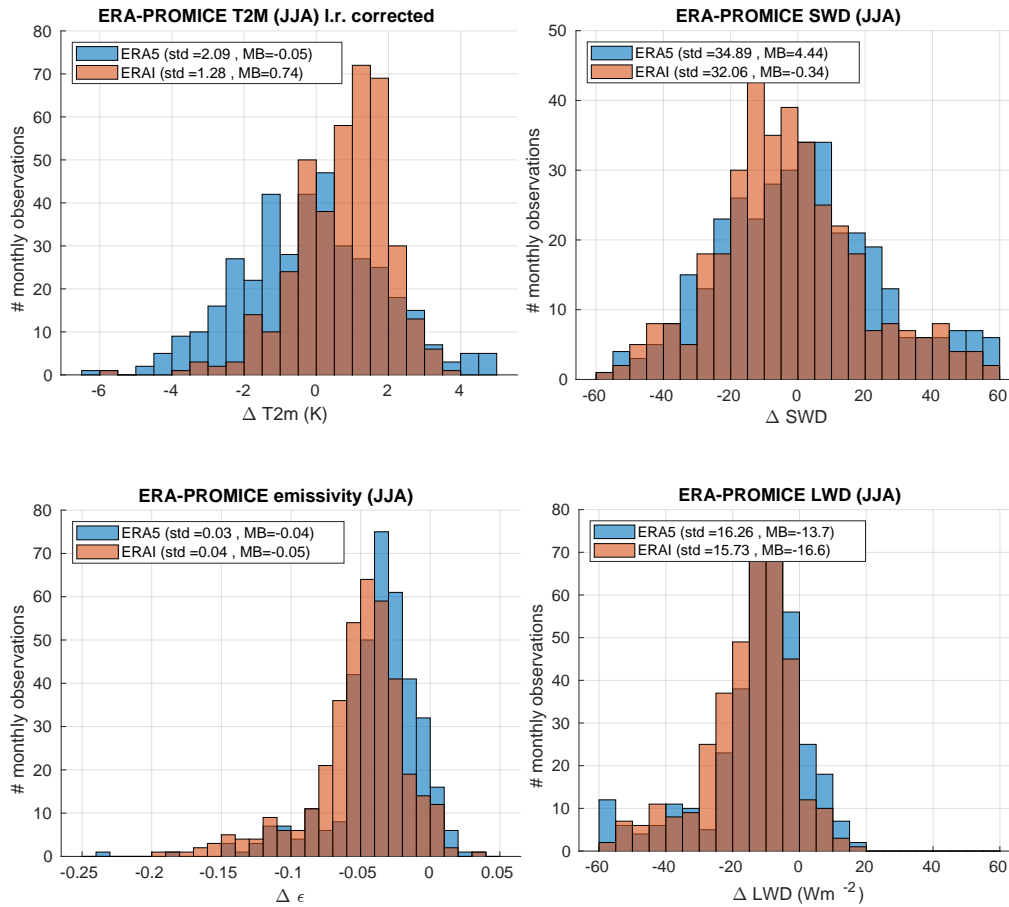
Figure 2. Distribution of ERA5 and ERAI biases with respect to monthly PROMICE observations for the summer months (June, July, August) in 2007–2016: 2m-air temperature (upper left), downward shortwave radiation (upper right), emissivity (lower left) and downward longwave radiation (lower right). The text box insets provide standard deviation (std) and mean biases (MB) for the respective distributions.

SWD data. In case of LWD both bias and spread can be reduced by recalculating LWD from emissivity and lapse rate corrected T2m (Supplement Fig. S9).

Over the lower parts of the ice sheet ($< 2000\,\mathrm{m}$), differences are pronounced, as shown by the temporal evolution of the fields considered (Fig. 3). In Fig. 3 height range covers the ablation zone which is generally limited to altitudes below $2000\,\mathrm{m}$ above sea level, analysis in $(1000\,\mathrm{m})$ intervals from 0 to $(4000\,\mathrm{m})$ is provided in the supplement Figs S10-S13. The averaged lapse rate corrected ERA5-ERAI 2m-air temperature difference here varies around a mean of $-1.0\,\mathrm{K}$ with a standard deviation of $0.24\,\mathrm{K}$ (Fig. 3). This bias is enhanced by $25\,\%$ during the period between 2002–2009 when it is consistently above $-1.25\,\mathrm{K}$. This colder period in ERA5 may be partly related to a known cold bias of ERA5 in the lower stratosphere between 2002 and 2006 (one reason why ECMWF released ERA5.1, a rerun of this period Simmons et al. (2020)). The mean bias for SWD varies around $16.7,\ \mathrm{W\,m^{-1}}$ with a standard deviation of $1.6,\ \mathrm{W\,m^{-1}}$ and for LWD varies around $6.9,\ \mathrm{W\,m^{-1}}$ with a standard
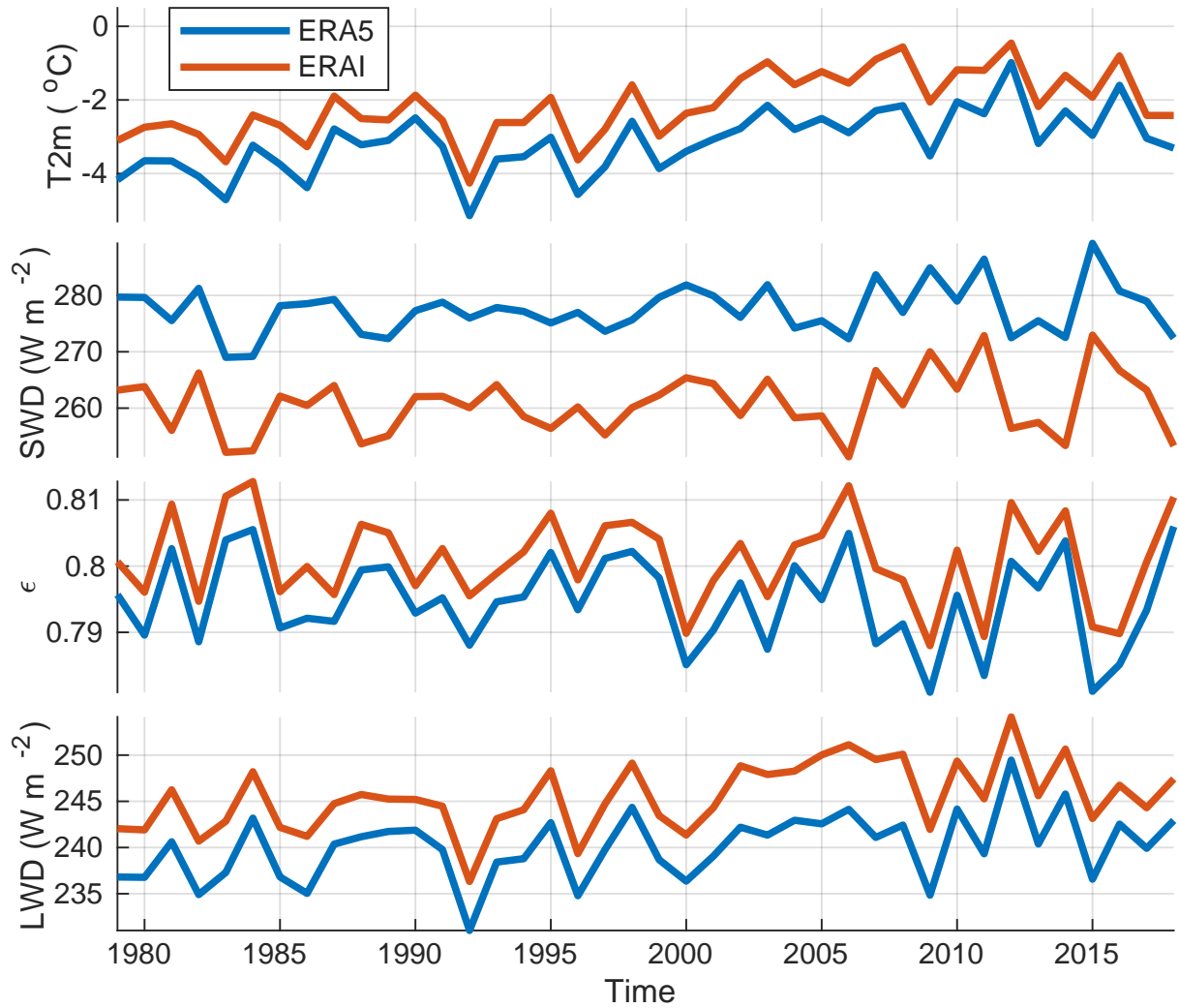
Figure 3. 1979–2016 yearly summer means of interpolated (a) lapse rate corrected 2m-air temperature, (b) downward surface shortwave radiation, (c) emissivity, and (d) downward longwave radiation for ERA5 (blue) and ERAI (red) averaged over the $0\,\mathrm{m}$ to $2000\,\mathrm{m}$ elevation range of the GrIS.

deviation of 1.1, $\mathrm{W\,m^{-1}}$. Differences in effective emissivity also remain largely stable over time, with a mean bias of -0.0063 and a standard deviation of 0.0017.

These biases in the ablation zone imply that using either ERAI or ERA5 climate to drive the same energy balance model will result in different surface melt rate distributions in GrIS. We use the simplified formulation of the surface energy balance for a melting snow surface as given in Krebs-Kanzow et al. (2018) to estimate the resulting melt rate difference as about

$$\Delta M = \left((1-A)\,\Delta SWD + k_1\,\Delta T2m\right)\,\frac{1}{\rho\,L_f}, \tag{3}$$

where A is the albedo of the surface, $\rho = 1000\,\mathrm{kg\,m^{-3}}$ is density of water, $L_f = 3.34 \times 10^5\,\mathrm{J\,kg^{-1}}$ is latent heat of fusion, and the parameter k_1 is chosen to be $10\,\mathrm{W\,K^{-1}\,m^{-2}}$. The differences between ERA5 and ERAI of $\Delta SWD = 15\,\mathrm{W\,m^{-2}}$ and $\Delta T2m = -1\,\mathrm{K}$ yield a range from $\Delta M = -0.25\,\mathrm{mm\,day^{-1}}$ for a low albedo of $A = 0.4$ in the dark bare ice zone to $-2\,\mathrm{mm\,day^{-1}}$ for a fresh snow albedo of $A = 0.9$. Therefore, melt rates from ERA5 are expected to remain mostly lower than the respective estimates based on ERAI, especially at higher altitudes where albedo is generally high. This would result in a lower equilibrium line and stronger melt gradients between the equilibrium line and the ice sheet's margin. However, stronger SWD differences may overcompensate for the lower temperatures in the darker parts of the ablation zone and consequently lead to stronger melt estimates under ERA5 forcing.

4 Discussion and conclusion

Our comparison reveals substantial, spatially and temporally coherent differences between ERA5 and ERA-Interim, resulting in a modified surface energy balance over the GrIS. ERA5 is characterized by systematically lower near-surface air temperatures and more intense insolation in summer. To some degree differences can be related to the higher spatial resolution of ERA5. In case of near surface air temperature small scale, resolution dependent differences can be removed largely by a uniform lapse rate correction while large scale differences of the order of $\Delta T2m = -1\,\mathrm{K}$ remain and appear unrelated to resolution differences. The difference in downware shortwave radiation (SWD) is particularly pronounced along the ice sheet's margins and may in part be related to the higher spatial resolution of ERA5 and a sharper transition of cloud properties from the coastal zone to the interior ice sheet. However, differences in downward shortwave radiation do not generally correspond to differences in atmospheric emissivity which indicates differences between the two reanalyses in cloud parameterization or radiation scheme.

Correcting the near-surface air temperatures with a lapse rate of $-5\,\mathrm{K\,km^{-1}}$ not only reduces the differences between the two reanalysis products but also improves the comparison with monthly observations from PROMICE weather stations for both data sets too. This result is consistent with slope lapse rates diagnosed from both data sets and stresses the benefit of this simple downscaling method when dealing with coarse-resolution temperature fields.

In contrast to Delhasse et al. (2020), we find a significant warm bias of ERAI relative to weather station data, but this is only fully evident when a lapse rate correction is applied, while SWD appears to be slightly overestimated in ERA5.

The observed differences between ERA5 and ERAI have implications for the estimation of surface melt and ultimately the release of runoff. Replacing ERAI with ERA5 forcing in an energy balance model of the GrIS may therefore require some re-calibration to reproduce existing observations (e.g., Shepherd et al., 2020).

Code and data availability. The reanalysis data sets are provided by the European Centre for Medium-Range Weather Forecasts (ECMWF). Information about ERA-Interim and ERA5 are given at https://www.ecmwf.int/en/forecasts/dataset/ecmwf-reanalysis-interim [accessed 2021-11-12] and https://www.ecmwf.int/en/forecasts/dataset/ecmwf-reanalysis-v5 [accessed 2021-11-12]

.

Author contributions. UKK performed the analysis and lead the manuscript writing. All authors contributed to the interpretation of the results and proofreading of the manuscript.

Competing interests. The authors declare that they have no conflict of interest.

Acknowledgements. U. Krebs-Kanzow acknowledges the Helmholtz Climate Initiative REKLIM (Regional Climate Change) and the research program PoF IV "Changing Earth – Sustaining our Future" of the Alfred Wegener Institute. C. Rodehacke has received funding from the European Union's Horizon 2021 research and innovation programme under grant agreement No 101056939 for the project RESCUE, and he has also received funding via the Alfred Wegener Institute's PACES2 research program.

References

Ahlstrom, A. P., Gravesen, P., Andersen, S. B., van As, D., Citterio, M., Fausto, R. S., Nielsen, S., Jepsen, H. F., Kristensen, S. S., Christensen, E. L., Stenseng, L., Forsberg, R., Hanson, S., Petersen, D., and Team, P. P.: A new programme for monitoring the mass loss of the Greenland ice sheet, Geological Survey of Denmark and Greenland Bulletin, pp. 61–64, 2008.

Born, A., Imhof, M. A., and Stocker, T. F.: An efficient surface energy-mass balance model for snow and ice, Cryosphere, 13, 1529–1546, https://doi.org/10.5194/tc-13-1529-2019, 2019.

Delhasse, A., Kittel, C., Amory, C., Hofer, S., van As, D., S. Fausto, R., and Fettweis, X.: Brief communication: Evaluation of the near-surface climate in ERA5 over the Greenland Ice Sheet, The Cryosphere, 14, 957–965, https://doi.org/10.5194/tc-14-957-2020, 2020.

Erokhina, O., Rogozhina, I., Prange, M., Bakker, P., Bernales, J., Paul, A., and Schulz, M.: Dependence of slope lapse rate over the Greenland ice sheet on background climate, Journal of Glaciology, 63, 568–572, https://doi.org/10.1017/jog.2017.10, 2017.

Fausto, R. S., van As, D., Mankoff, K. D., Vandecrux, B., Citterio, M., Ahlstrøm, A. P., Andersen, S. B., Colgan, W., Karlsson, N. B., Kjeldsen, K. K., Korsgaard, N. J., Larsen, S. H., Nielsen, S., Pedersen, A. Ø., Shields, C. L., Solgaard, A. M., and Box, J. E.: Programme for Monitoring of the Greenland Ice Sheet (PROMICE) automatic weather station data, Earth System Science Data, 13, 3819–3845, https://doi.org/10.5194/essd-13-3819-2021, 2021.

Fettweis, X., Hofer, S., Krebs-Kanzow, U., Amory, C., Aoki, T., Berends, C. J., Born, A., Box, J. E., Delhasse, A., Fujita, K., Gierz, P., Goelzer, H., Hanna, E., Hashimoto, A., Huybrechts, P., Kapsch, M.-L., King, M. D., Kittel, C., Lang, C., Langen, P. L., Lenaerts, J. T. M., Liston, G. E., Lohmann, G., Mernild, S. H., Mikolajewicz, U., Modali, K., Mottram, R. H., Niwano, M., Noël, B., Ryan, J. C., Smith, A., Streffing, J., Tedesco, M., van de Berg, W. J., van den Broeke, M., van de Wal, R. S. W., van Kampenhout, L., Wilton, D., Wouters, B., Ziemen, F., and Zolles, T.: GrSMBMIP: intercomparison of the modelled 1980–2012 surface mass balance over the Greenland Ice Sheet, The Cryosphere, 14, 3935–3958, https://doi.org/10.5194/tc-14-3935-2020, 2020.

Hanna, E., Cappelen, J., Fettweis, X., Mernild, S. H., Mote, T. L., Mottram, R., Steffen, K., Ballinger, T. J., and Hall, R. J.: Greenland surface air temperature changes from 1981 to 2019 and implications for ice-sheet melt and mass-balance change, International Journal of Climatology, 41, E1336–E1352, https://doi.org/https://doi.org/10.1002/joc.6771, 2021.

King, J. C., Marshall, G. J., Colwell, S., Arndt, S., Allen-Sader, C., and Phillips, T.: The Performance of the ERA-Interim and ERA5 Atmospheric Reanalyses Over Weddell Sea Pack Ice, Journal of Geophysical Research-Oceans, 127, https://doi.org/10.1029/2022JC018805, 2022.

Krebs-Kanzow, U., Gierz, P., and Lohmann, G.: Brief communication: An ice surface melt scheme including the diurnal cycle of solar radiation, The Cryosphere, 12, 3923–3930, https://doi.org/10.5194/tc-12-3923-2018, 2018.

Krebs-Kanzow, U., Gierz, P., Rodehacke, C. B., Xu, S., Yang, H., and Lohmann, G.: The diurnal Energy Balance Model (dEBM): a convenient surface mass balance solution for ice sheets in Earth system modeling, The Cryosphere, 15, 2295–2313, https://doi.org/10.5194/tc-15-2295-2021, 2021.

Morlighem, M., Rignot, E., Mouginot, J., Seroussi, H., and Larour, E.: Deeply incised submarine glacial valleys beneath the Greenland ice sheet, Nature Geoscience, 7, 418–422, https://doi.org/10.1038/NGEO2167, 2014.

Climate Change (IPCC), I. P.: Future Global Climate: Scenario-based Projections and Near-term Information, p. 553–672, Cambridge University Press, https://doi.org/10.1017/9781009157896.006, 2023.

Shepherd, A., Ivins, E., Rignot, E., Smith, B., van den Broeke, M., Velicogna, I., Whitehouse, P., Briggs, K., Joughin, I., Krinner, G., Nowicki, S., Payne, T., Scambos, T., Schlegel, N., A, G., Agosta, C., Ahlstrom, A., Babonis, G., Barletta, V. R., Bjork, A. A., Blazquez, A., Bonin,

J., Colgan, W., Csatho, B., Cullather, R., Engdahl, M. E., Felikson, D., Fettweis, X., Forsberg, R., Hogg, A. E., Gallee, H., Gardner, A., Gilbert, L., Gourmelen, N., Groh, A., Gunter, B., Hanna, E., Harig, C., Helm, V., Horvath, A., Horwath, M., Khan, S., Kjeldsen, K. K.,
190   Konrad, H., Langen, P. L., Lecavalier, B., Loomis, B., Luthcke, S., McMillan, M., Melini, D., Mernild, S., Mohajerani, Y., Moore, P., Mottram, R., Mouginot, J., Moyano, G., Muir, A., Nagler, T., Nield, G., Nilsson, J., Noel, B., Otosaka, I., Pattle, M. E., Peltier, W. R., Pie, N., Rietbroek, R., Rott, H., Sorensen, L. S., Sasgen, I., Save, H., Scheuchl, B., Schrama, E., Schroeder, L., Seo, K.-W., Simonsen, S. B., Slater, T., Spada, G., Sutterley, T., Talpe, M., Tarasov, L., van de Berg, W. J., van der Walt, W., van Wessem, M., Vishwakarma, B. D., Wiese, D., Wilton, D., Wagner, T., Wouters, B., Wuite, J., and Team, I.: Mass balance of the Greenland Ice Sheet from 1992 to 2018,
195   Nature, 579, 233+, https://doi.org/10.1038/s41586-019-1855-2, 2020.

Simmons, A., Soci, C., Nicolas, J., Bell, B., Berrisford, P., Dragani, R., Flemming, J., Haimberger, L., Healy, S., Hersbach, H., Horányi, A., Inness, A., Munoz-Sabater, J., Radu, R., and Schepers, D.: Global stratospheric temperature bias and other stratospheric aspects of ERA5 and ERA5.1, https://doi.org/10.21957/rcxqfmg0, 2020.

Wang, C., Graham, R. M., Wang, K., Gerland, S., and Granskog, M. A.: Comparison of ERA5 and ERA-Interim near-surface air tempera-
200   ture, snowfall and precipitation over Arctic sea ice: effects on sea ice thermodynamics and evolution, The Cryosphere, 13, 1661–1679, https://doi.org/10.5194/tc-13-1661-2019, 2019.